Journal of Crystal Growth 311 (2009) 4102–4108

Contents lists available at ScienceDirect

Journal of Crystal Growth

journal homepage: www.elsevier.com/locate/jcrysgro

The effect of cooling rate during hydrothermal synthesis of ZnO nanorods

Raluca Savu [a,*], Rodrigo Parra [a,b], Ednan Joanni [a], Boštjan Jančar [c], Sayonara A. Eliziário [a], Rorivaldo de Camargo [d], Paulo R. Bueno [a], José A. Varela [a], Elson Longo [a], Maria A. Zaghete [a]

[a] Instituto de Química—UNESP Araraquara, Rua Francisco Degni s/n, 14800-900 Araraquara, SP, Brazil
[b] Instituto de Investigaciones en Ciencia y Tecnología de Materiales (INTEMA), CONICET-UNMdP, B7608FDQ Mar del Plata, Argentina
[c] Advanced Materials Department, Jozef Stefan Institute, Jamova 39, 1000 Ljubljana, Slovenia
[d] Departamento de Química, UFSCar, Washington Luiz km 235, 13565-905 São Carlos, SP, Brazil

ARTICLE INFO

Article history:
Received 19 May 2009
Received in revised form
14 June 2009
Accepted 17 June 2009
Communicated by P. Rudolph
Available online 27 June 2009

PACS:
78.30.Fs
61.46.w
73.50.Pz
81.16.Be

Keywords:
A1. Crystal morphology
A2. Growth from solutions
B1. Nanomaterials
B2. Semiconducting II–VI materials

ABSTRACT

The hydrothermal method was employed in order to obtain zinc oxide nanorods directly on $Si/SiO_2/Ti/Zn$ substrates forming brush-like layers. In the final stages of synthesis, the reaction vessel was naturally cooled or submitted to a quenching process. X-ray diffraction results showed that all the nanostructures grew [0 0 0 1] oriented perpendicular to the substrate. The influence of the cooling process over the morphology and dimensions of the nanorods was studied by scanning electron microscopy. High-resolution transmission electron microscopy images of the quenched samples showed that the zinc oxide (ZnO) crystal surfaces exhibit a thin-layered coating surrounding the crystal with a high degree of defects, as confirmed by Raman spectroscopy results. Photodetectors made from these samples exhibited enhanced UV photoresponses when compared to the ones based on naturally cooled nanorods.

1. Introduction

Ever since the discovery of carbon nanotubes [1], developments in nanotechnology have led to the synthesis of semiconducting oxide nanostructures. The increasing interest in nanoscale structures can be attributed to their unique optical and electrical properties due to quantum confinement effects and high surface-to-volume ratios, with great prospect of applying them as building blocks in electronic and photonic devices [2–5]. The methods reported for the synthesis of semiconducting oxide nanowires include chemical bath deposition [5–8], hydrothermal synthesis [9–13], chemical vapor deposition [14,15], thermal evaporation [16,17] and sputtering [18,19]. Hydrothermal synthesis is often used because it allows control of size, morphology and crystallinity by tuning of the experimental variables. Another attractive feature is the possibility of performing in-situ growth of films directly from aqueous precursors in solution by introducing the substrates inside the reacting medium [20].

Zinc oxide (ZnO) is one of the most exploited semiconductors due to its intrinsic properties, like the wide direct band-gap (3.37 eV), large exciton binding energy (60 meV) and excellent chemical and thermal stability, allowing its use in optoelectronic devices [5]. Boyle et al. studied the influence of different substrates and counter-ions on the growth of oriented ZnO nanorods in aqueous solutions of zinc nitrate and hexamethylenetetramine (HMTA) [21]. Yamabi et al. studied the growth of wurtzite films onto several substrates and found that the nucleation of nanowires is strongly dependant on the pH [22]. In addition, Guo et al. showed the enhanced growth of oriented nanorods and/or nanowires by using catalyst layers, which substrate increases the substrate coverage density of the nanostructures due to the availability of ZnO crystal seeds for nucleation [23].

HMTA, widely used in the hydrothermal synthesis of ZnO nanorods, nanowires and acicular nanocrystals [20–25], forms stable hydrogen-bonded 3D complexes with many transition metals in which it is not directly bonded to the metal but to coordinated water by means of hydrogen bonds that sustain the resulting framework [6]. Such species might contribute or facilitate the crystallization of ZnO into nanorod or nanowire

* Corresponding author.
E-mail address: raluk1978@yahoo.com (R. Savu).

0022-0248/$ - see front matter © 2009 Elsevier B.V. All rights reserved.
doi:10.1016/j.jcrysgro.2009.06.039

structures. On the other hand, because of its low basicity and relatively weak metal-complexing properties, it might only act as a pH buffer and, therefore, it would not determine the final crystallite morphology. As it decomposes into formaldehyde and ammonia with increasing temperature, OH^- species are released to the medium promoting the precipitation of the metal hydroxide and/or oxide [24]. Considering this, further systematic studies are necessary in order to clarify the role of HMTA.

The ZnO crystalline morphology is determined by a great number of variables such as additives (amines, acids and surfactants), counter-ion, concentration of reactants and temperature. However, the cooling rate of the system is one of the main variables of the hydrothermal process and studies on its control and effects are not available in the literature. Hitherto, there are serious problems in achieving good cooling control without complex laboratory equipment. In this work, we present a discussion of the in-situ growth of nanostructured ZnO coatings obtained by hydrothermal synthesis in mild conditions and the effect of the cooling rate over the morphology and properties of nanorods.

2. Experimental procedure

Oxidized silicon substrates coated with Ti/Zn thin films were used for the hydrothermal synthesis of ZnO nanorods. Prior to the sputtering deposition of the catalyst layers, the substrates were washed with ethanol, acetone and isopropanol and blown with dry nitrogen. Room-temperature RF and DC sputtering were performed in order to deposit a 15 nm Ti buffer layer and 50 nm of Zn catalytic thin film, respectively.

ZnO nanostructures were grown using aqueous solutions of zinc nitrate ($Zn(NO_3)_2 \cdot 6H_2O$) and HMTA as precursors. The reagents were dissolved in distilled water at room temperature, with the template solution being slowly added to the zinc solution under continuous stirring. The resulting transparent solution was placed in a polytetrafluorethylene (PTFE)-lined stainless steel pressure vessel. The substrates were suspended in the solution with the zinc-coated surface facing the bottom of the flask. The hydrothermal process was performed in a hot Vaseline bath at 110 °C for a 6 h synthesis time under continuous stirring of solution. The pressure vessel was then removed from the hot bath and allowed to cool down naturally (in air) or immersed in a room-temperature Vaseline bath in order to increase the heat-transfer rate. After 1 min immersed in the room-temperature Vaseline bath, the final temperature reached was of 50 °C. The nanostructured deposits were washed several times with distilled water and ethanol and dried in an oven at 75 °C.

The goal of this study is to observe the influence of the cooling process over the morphology and crystallinity of the nanostructures. Changes in the zinc salt, template solutions and molar concentration ratios were also carried out in order to see the influence of all these variables over the growth and properties of the resulting nanostructures. The complete set of parameters used in the process is presented in Table 1.

Table 1
Complete set of parameters used for the hydrothermal process.

Sample name	Zn (mol/L)	HMTA (mol/L)	pH	Cooling
ZO1	0.055	0.01	6.65	Natural
ZO2	0.055	0.01	6.65	Quenched
ZO3	0.0275	0.1	6.5	Natural
ZO4	0.0275	0.1	6.5	Quenched
ZO5	0.055	0.1	6.95	Natural
ZO6	0.055	0.1	6.95	Quenched

X-ray diffraction (XRD, Rigaku Rint 2000) scans were performed in order to assess the crystalline structure of the nanostructured films and their orientation. The influence of the cooling process over the morphology and dimensions of the nanorods was studied by field emission scanning electron microscopy (FE-SEM, Zeiss Supra 35). High-resolution transmission electron microscopy (HR-TEM, Jeol JEM 2100) and selected area electron diffraction (SAED) were performed on individual nanorods, naturally cooled or quenched, in order to determine the growth direction and the influence of the cooling rate over the degree of cristallinity of the nanostructures. Raman spectroscopy measurements were carried out at room temperature using a Bruker RFS/100 spectrometer. A 1064 nm Nd:YAG laser was used as excitation source with its power kept at 80 mW. In order to perform the electrical measurements, 150-nm-thick and 172-μm-diameter sputtered platinum electrodes were deposited on the samples. The UV response of the nanostructured films was registered at room temperature using an Hg vapor lamp. The measurements were performed with a Solartron SI1287A electrochemical interface, applying a 5 V potential difference and a light intensity of 2.4 mW/cm^2.

3. Results and discussion

Fig. 1 shows FE-SEM surface and cross-section images of the naturally cooled (Fig. 1a and b) and quenched (Fig. 1c and d) nanostructured films obtained using the precursor based on the highest zinc nitrate molar concentration (0.055 M) with 0.01 M HMTA. The naturally cooled rods exhibit a very good hexagonal shape, having approximately 150 nm in diameter (Inset Fig. 1a) and around 3.4 μm in length (Fig. 1b).

The morphology is well preserved along the body of the nanostructures, with the samples having a high substrate coverage density. For the quenched sample the substrate coverage is maintained as can be observed in Fig. 1c.

The main difference between the two samples is in the morphology and dimensions of the rods. For the rapidly cooled sample, a value of approximately 120 nm (Inset Fig. 1c) is reached at the tip of the nanostructure, with the nanorods tapering along their length. The hexagonal shape is not so well defined and the nanostructures are shorter, having approximately 2.5 μm in length (Fig. 1d). Along with these characteristics, one can notice the existence of very small pointed tips in the nanorods (Inset Fig. 1c), which can be attributed to the different cooling processes. Clearly, the discontinuity in the thermal energy supply lead to a decrease in the rate of dissolution/recrystallization during the cooling stage, typical of the hydrothermal process [26,27] and, as a consequence, to a smaller mean crystal size and a decrease in the degree of crystallization and morphological perfection of the nanorods.

Fig. 2 presents the FE-SEM images of the nanostructures obtained from the 0.0275 M $Zn(NO_3)_2 \cdot 6H_2O$ and 0.1 M HMTA precursor solution. The naturally cooled sample is shown in Fig. 2a and b and the one submitted to the faster cooling process in Fig. 2c and d. The substrate coverage is still maintained, with the films being formed by much thinner (Fig. 2a and c) and shorter (Fig. 2b and d) nanorods when compared to the previous samples. This can be attributed to the decrease in the Zn^{2+} concentration, being consistent with the results reported in the literature by other researchers [23]. The nanorods composing the ZO3 sample exhibit a relatively constant cross-section along the length, having approximately 100 nm diameter and 1.8 μm length. Compared to the ZO3 sample, the nanostructured film submitted to the quenched cooling process exhibits nanorods with a very poor hexagonal shape (inset Fig. 2c). In addition, the nanowires present

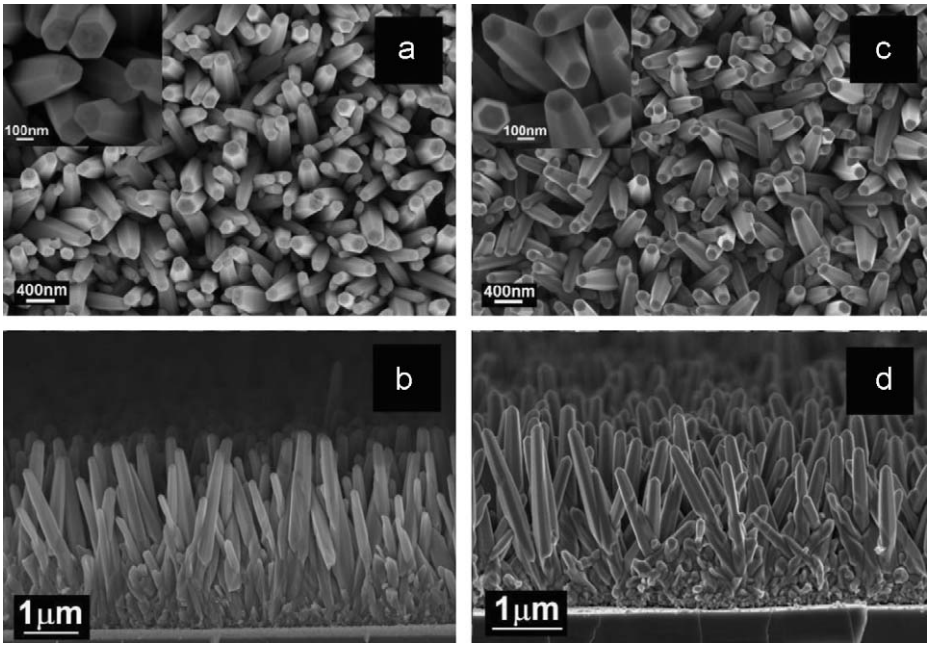

Fig. 1. FE-SEM images of the ZO1 (a and b) and ZO2 (c and d) samples obtained from the precursor with the highest zinc nitrate concentration and 0.01 M HMTA. The insets in (a) and (c) present higher-resolution surface images of the nanorods.

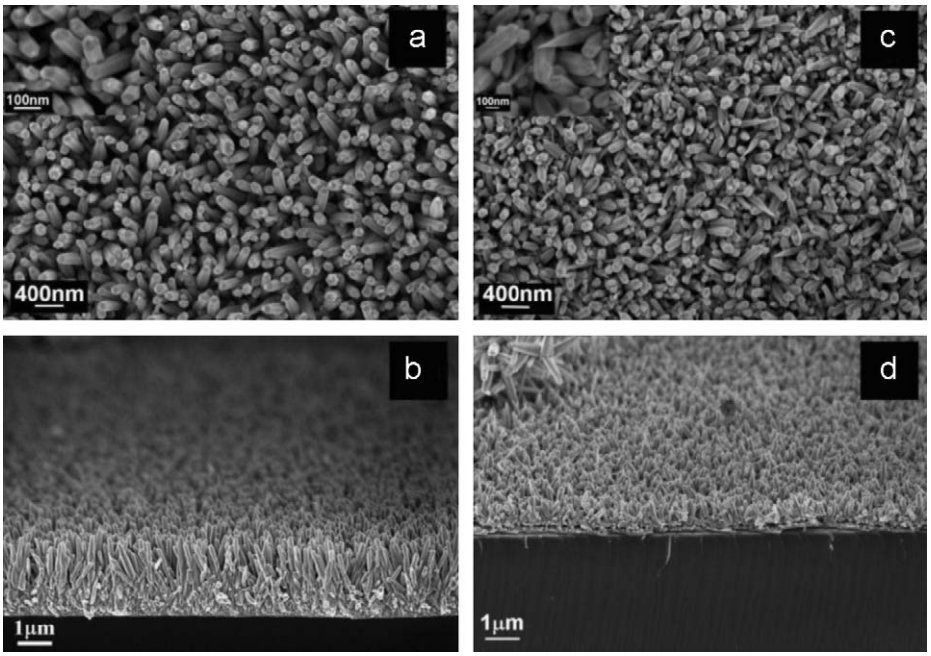

Fig. 2. Surface and cross-section FE-SEM images of the ZO3 (a and b) and ZO4 (c and d) nanorods obtained using 0.0275 M zinc nitrate solution and the highest HMTA concentration. The insets show higher-resolution surface images revealing the differences in morphology of the nanorods without (a) and with (c) quenching.

a length of about 500 nm and are thinner than 100 nm, with no possibility of a more precise evaluation due to the variable rod diameters.

Fig. 3 shows the FE-SEM images of the naturally cooled (Fig. 3a and b) and quenched (Fig. 3c and d) samples obtained from the most concentrated solution (ZO5 and ZO6, respectively). In both cases, the nanostructures exhibit a very similar substrate coverage density, but obviously the changes in the cooling rate greatly affected their morphology and length. For the naturally cooled sample, the rods have approximately 5 μm length with very few surface defects (Fig. 3b), tapering along the length and exhibiting pointed tips (Fig. 3a). Compared to the naturally cooled one, the quenched sample displays nanorods with broken and/or hollow large tips of approximately 250 nm and half the length of the ZO5 nanostructures (2.5 μm). Looking at the FE-SEM images (Fig. 3c and d) it can be observed that the rapidly cooled sample presents a large number of imperfect wires with many defects and with a poorly defined hexagonal cross-section. Comparing the two samples shown in Fig. 3, it is clear that for the quenched one the crystallization was drastically reduced once the reactor was immersed in the room-temperature Vaseline bath. Once more, this is an indication that the discontinuity in the thermal energy

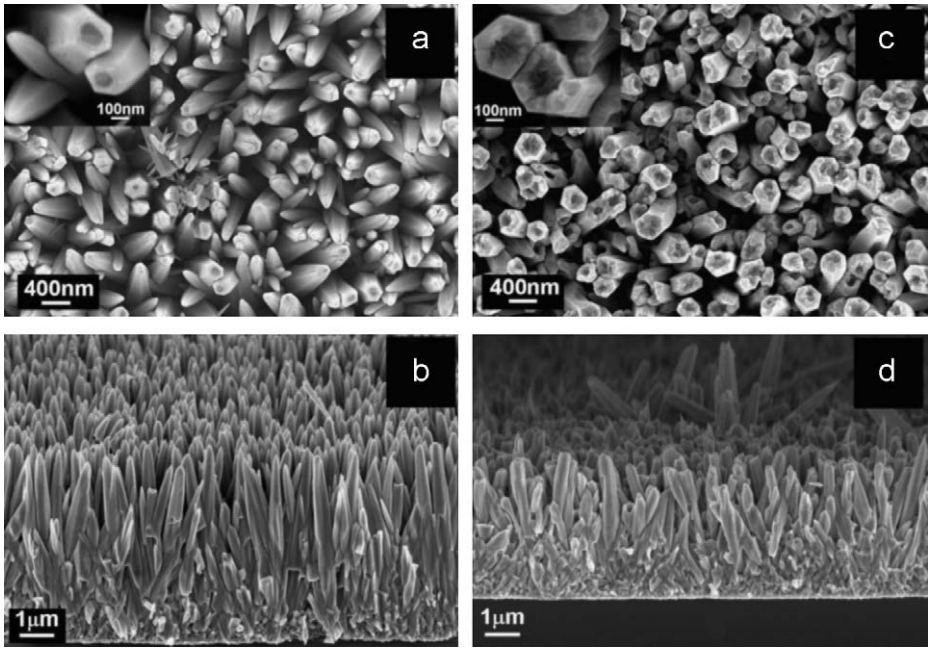

Fig. 3. FE-SEM images of the samples naturally cooled (a and b) and quenched (c and d) obtained from the most concentrated solution, samples ZO5 and ZO6, respectively. The insets in (a) and (c) present higher-resolution surface images of the nanorods composing the two samples.

supply led to a faster cooling, impairing the crystallization process and consequently the morphological make-up of the nanorods.

Comparing Figs. 1 and 3, one can easily observe that when the concentration of template was increased, thicker and longer nanorods were obtained. Moreover, when comparing the two quenched samples using these two sets of synthesis parameters, one can observe that while the rods composing the ZO2 sample are better defined and less defective, with small and pointed tips, the ZO6 nanostructures exhibit hollow, irregular tips with a poorly defined hexagonal shape. This indicates that, for the sample with the smallest HMTA molar concentration, the 6 h synthesis time was sufficient to complete the crystallization, giving rise to better-defined rods, while for the highest HMTA concentration this process was still occurring when the temperature was reduced, leading to rods with larger, irregular tips. When a synthesis was performed using only the zinc salt, without any template (results not shown here), no nanorods were formed on the substrate and irregularly shaped nanocrystals were obtained. This result confirms the important role of HMTA in the formation of nanorod or nanowire-shaped ZnO crystals.

Vayssieres [20] reported that, in order to reduce the diameter of the nanostructures, a viable strategy is to reduce the overall concentration of the reactants, while keeping the ratio of Zn^{2+} to amine constant at 1:1. In our study, when the zinc nitrate molar concentration was halved (keeping the HMTA concentration at 0.1 M), thinner and shorter nanorods were obtained (Fig. 2). These results are in agreement with those reported by Guo et al. [23]. In their report, a very detailed study of the influence of the experimental parameters (catalytic layer, temperature, time, etc.) over the growth and morphology of the ZnO nanostructures was carried out, but no reference was made to the cooling process used. Our FE-SEM results indicate that the cooling rate is a very important parameter to be controlled.

As this last set of samples provided a more clear evidence of the difference between the two cooling processes, further characterizations were performed in order to evaluate the influence of the cooling rate over the cristallinity and properties of the nanostructures.

Fig. 4a and b shows TEM images of nanorods from a naturally cooled sample (ZO5) and Fig. 4c and d from a quenched one (ZO6). As can be noticed in Fig. 4a, the naturally cooled rod has a hexagonal structure (wurtzite ZnO). This result is also confirmed by HR-TEM (Fig. 4b) and SAED analyses (Inset Fig. 4a). In contrast, it is evident that, besides the poor hexagonal shape and surface defects, the quenched nanorod (Fig. 4c) exhibits a thin coating structure surrounding the crystal, being more evident at the tip. The surface of the quenched sample exhibits a considerable amount of pits and irregularities, when compared to the naturally cooled one, indicating a higher degree of defects. The TEM characterization corroborates the FE-SEM results, indicating once more that the crystallization process was affected by the rapid cooling of the ZO6 sample. The HR-TEM images of the quenched sample (Fig. 4d) show that the edges of the ZnO crystal surface are composed by a thin-layered structure. The SAED patterns for both the naturally cooled rod (Inset Fig. 4a) and the quenched one (Inset Fig. 4b) indicate the growth direction as being [0 0 0 1]. The properties of the nanostructures are highly surface dependent; therefore the degree of surface cristallinity should affect the performance of devices built from those nanostructures. A common example is the level of photoluminescence measured for nanostructures with different concentrations of defects [7,23].

Fig. 5 shows the XRD patterns of the ZO5 and ZO6 highly oriented nanorod arrays, Fig. 5a and b, respectively. All the peaks present in the diagram are indexed to the wurtzite crystalline structure of zinc oxide (JCPDS card no. 36-1451). The higher intensity obtained for the (0 0 0 2) diffraction peak, when compared to the relative intensity of the $(10\bar{1}1)$ plane that is usually correlated to the maximum intensity peak of ZnO, indicates the anisotropic growth of the nanorods in the [0 0 0 1] direction, perpendicular to the substrate, confirming the HR-TEM findings.

Fig. 6 shows the Raman spectra of the naturally cooled (a) and submitted to the quenching process (b) ZnO nanorods obtained from the most concentrated solution. In both graphs, the peak observed near 520 cm^{-1} is due to the silicon substrate. For the

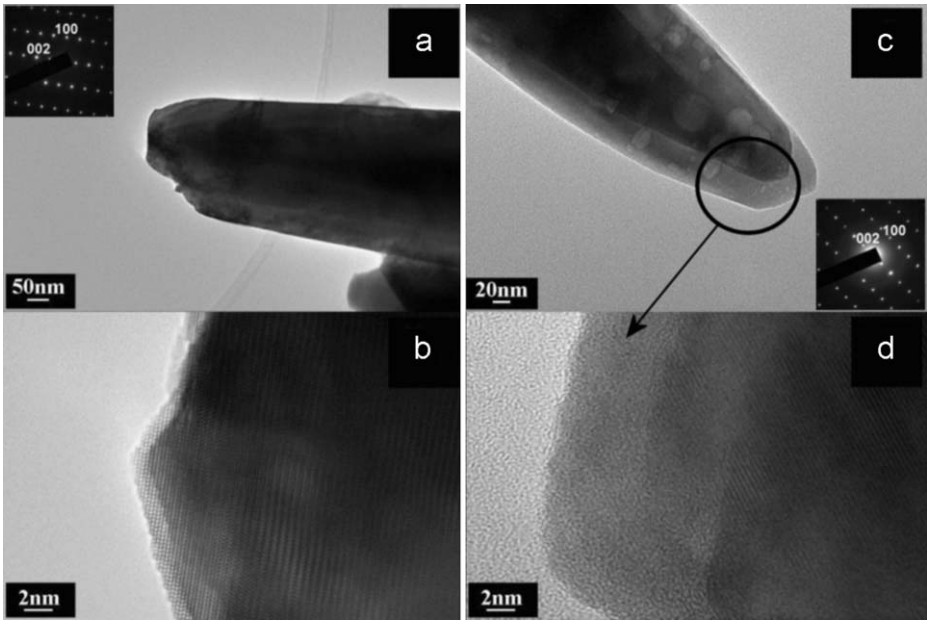

Fig. 4. TEM images of the naturally cooled (a and b) and quenched (c and d) nanorods obtained from the most concentrated solution. The insets present the SAED patterns taken on these nanostructures.

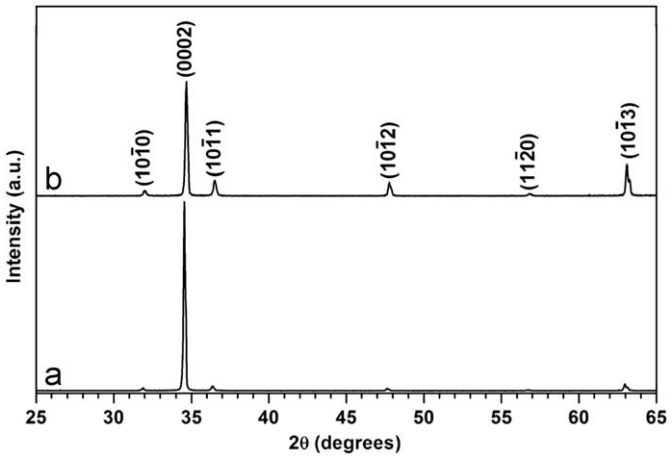

Fig. 5. X-ray diffraction patterns of ZO5 (a) and ZO6 (b) samples.

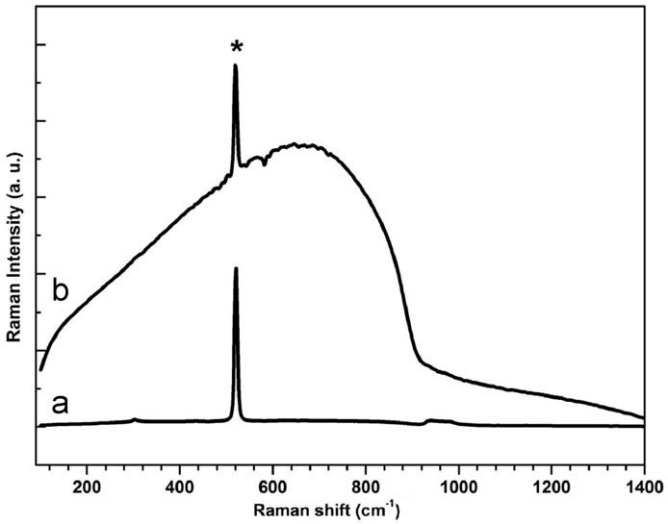

Fig. 6. Raman spectra of naturally cooled (a) and quenched (b) ZnO nanorod arrays obtained from the most concentrated precursor. The substrate peak is marked with the * symbol.

naturally cooled sample (Fig. 6a) only the peak from the silicon substrate is present, with no Raman peaks associated with specific ZnO vibration modes. However, this can be due to the high degree of order at long and short distances, as confirmed by the XRD and HR-TEM measurements, as well as to the small size of the nanostructures. For the quenched sample (Fig. 6b), a broad Raman band is observed, possibly because of disorder at short distance. This result confirms the HR-TEM characterization (Fig. 4c and d) that showed the existence of a thin-layered structure and defects at the surface of the nanorods. Lorentzian fits in the 100–1200 cm^{-1} Raman shift region were performed in order to visualize the peaks of the quenched sample. Bands located at about 365 and 458 cm^{-1} correspond to the A_1 and E_1 modes. The broad band at around 573 cm^{-1} is due to disorder-activated Raman scattering for the A_1 mode, results also confirmed by the literature [28]. These bands are associated with the first-order Raman active modes of the ZnO phase [29]. There is also other multi-phonon band at 750–820 cm^{-1} possibly due to small defects [30]. A larger, less intense Raman band, in the Raman shift region from 1150 to 1400 cm^{-1}, is attributed to the optical overtone and associated with the second-order Raman active modes [29].

Fig. 7 presents the UV response of the naturally cooled and quenched nanorods composing the sample sets ZO5/ZO6 (Fig. 7a) and ZO1/ZO2 (Fig. 7b), respectively. As already reported in the literature, the UV photoconductivity in ZnO is basically the result of two processes: one surface related and another bulk related [31]. The surface-related photoconductivity is due to the adsorption and desorption of chemisorbed oxygen at the surface of the ZnO nanorods, which acts as a depletion layer, while the bulk-related process is associated with the release, upon UV illumination, of the electrons trapped by the bulk deep defect states [31,32]. As expected, due to changes in the cooling process and consequently in the crystalline arrangement of the nanostructures, the quenched sample (Fig. 7a empty squares) presents a higher UV response when compared with the naturally cooled sample (Fig. 7a full squares). This can be attributed to the

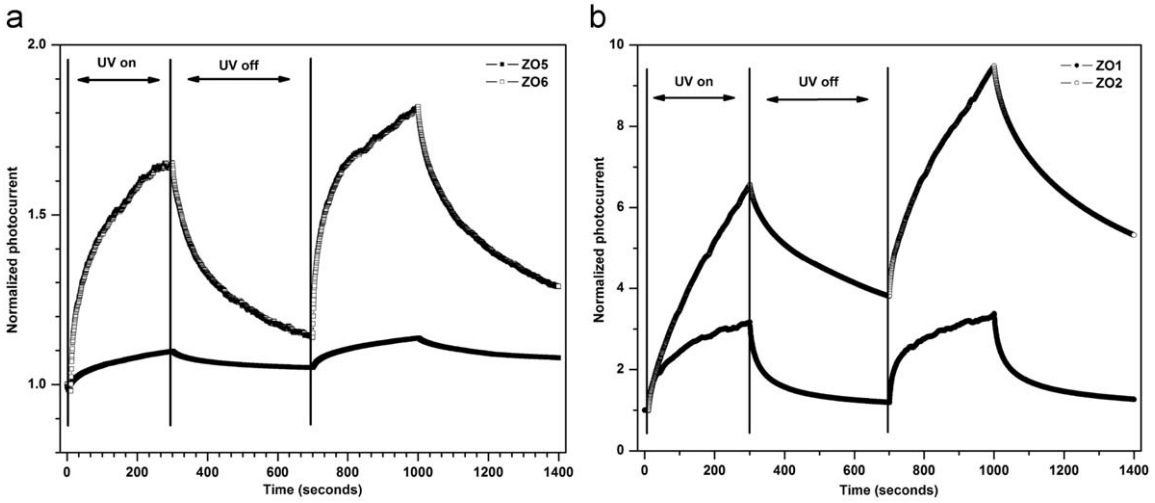

Fig. 7. UV photodetection response of the naturally cooled (filled symbols) and quenched (empty symbols) nanorods composing the sample sets ZO5/ZO6 (a) and ZO1/ZO2 (b).

existence of a higher amount of defects at the surface and in the bulk of the quenched nanorods, increasing both the surface and bulk contributions to the UV response. When compared to the other results in the literature [32], the response of our sensors is slow. This is probably due to the larger nanorod diameter as well as to the contribution of the continuous layer, much thicker than the one used by Bera and Basak [32]. The response of the quenched sample is almost three times more intense than the naturally cooled one indicating that, with a well-controlled cooling process, nanostructures with different morphologies and crystalline levels can be obtained, leading to enhanced properties. The same trend is followed by the sample set ZO1/ZO2, as can be noticed in Fig. 7b. The quenched sample (Fig. 7b empty dots) exhibit a much higher photocurrent when compared with the naturally cooled one (Fig. 7b filled dots). Moreover, when comparing both naturally cooled samples (samples ZO1 and ZO5, Fig. 7a and b, respectively), we can observe that, due to the smaller diameters, sample ZO1 shows a higher UV response than sample ZO5, indicating the bulk contribution to the UV response as well as the influence of the dimensions.

Another phenomenon, better observed in case of the quenched nanorods (empty symbols in Fig. 7a and b), after the UV light was turned off, is the persistent photoconductivity (PPC) as reported by Prades et al. [33]. The authors attributed this process to the surface built-in potential due to oxygen adsorption, which prevents the recombination of a fraction of the electron–hole pairs, leading to PPC after the UV light is turned off [33].

4. Conclusions

Hydrothermally synthesized ZnO nanorods with different morphologies and crystalline degrees were obtained by altering the cooling process, zinc concentration and zinc/template molar ratios. X-ray diffraction patterns showed that the nanorods grew oriented in the [0 0 0 1] direction, perpendicular to the substrate. FE-SEM and HR-TEM proved that the cooling process is an important parameter to be manipulated, considering its influence in the crystalline and morphological characteristics of the nanostructures. Because of a decrease in the crystallization process during quenching, randomly oriented crystalline clusters within an amorphous matrix are present in the surface layers of the nanorods. The UV response of quenched samples is almost three times higher than that of the naturally cooled ones indicating that nanostructures with different morphologies, crystalline levels and enhanced properties can be obtained with a well-controlled cooling process.

In our opinion, even though there is no quantification of the cooling rate, this study shows that this is another important parameter to be controlled during hydrothermal synthesis. The results reported in the literature by different workers can only be compared if the cooling rate used in the hydrothermal experiments is given, since otherwise identical experiments can lead to different results in terms of morphology and properties.

Acknowledgements

The authors acknowledge the financial support of the FAPESP and CNPq Brazilian foundations.

Appendix 1. Supporting Information

Supplementary data associated with this article can be found in the online version at doi:10.1016/j.jcrysgro.2009.06.039.

References

[1] S. Iijima, Nature 354 (1991) 65.
[2] C.N.R. Rao, F.L. Deepak, G. Gundiah, A. Govindaraj, Prog. Solid State Chem. 31 (2003) 5.
[3] P. Nguyen, H.T. Ng, T. Yamada, M.K. Smith, J. Li, J. Han, M. Meyyappan, Nano Letter 4 (2004) 651.
[4] M. Law, J. Goldberger, P. Yang, Annu. Rev. Mater. Res. 34 (2004) 83.
[5] W. Peng, S. Qu, G. Cong, Z. Wang, Cryst. Growth Des. 6 (2006) 1518.
[6] P. Afanasiev, S. Chouzier, T. Czeri, G. Pilet, C. Pichon, M. Roy, M. Vrinat, Inorg. Chem. 47 (2008) 2303.
[7] M. Wang, E.J. Kim, S.H. Hahn, C. Park, K.-K. Koo, Cryst. Growth Des. 8 (2008) 501.
[8] K. Govender, D.S. Boyle, P.B. Kenway, P.J. O'Brien, Mater. Chem. 14 (2004) 2575.
[9] M. Yang, G. Pang, L. Jiang, S. Feng, Nanotechnology 17 (2006) 206.
[10] M.N.R. Ashfold, R.P. Doherty, N.G. Ndifor-Angwafor, D.J. Riley, Y. Sun, Thin Solid Films 515 (2007) 8679.
[11] R. Zhang, S. Kumar, S. Zou, L.L. Kerr, Cryst. Growth Des. 8 (2008) 381.
[12] H. Qian, G. Lin, Y. Zhang, P. Gunawan, R. Xu, Nanotechnology 18 (2007) 355602.
[13] Y.-J. Lee, D.S. Ruby, D.W. Peters, B.B. McKenzie, J.W.P. Hsu, Nano Lett. 8 (2008) 1501.
[14] J.-J. Wu, S.-C. Liu, Adv. Mater. 14 (2002) 215.
[15] A.-J. Cheng, Y. Tzeng, Y. Zhou, M. Park, T.-H. Wu, C. Shannon, D. Wang, W. Lee, Appl. Phys. Lett. 92 (2008) 092113.
[16] Y. Wu, Z. Xi, J. Zhang, Q. Zhang, Mater. Chem. Phys. 110 (2008) 445.

[17] T.-J. Hsueh, C.-L. Hsu, S.-J. Chang, I.-C. Chen, Sens. Actuators B 126 (2007) 473.
[18] R. Teki, T.C. Parker, H. Li, N. Koratkar, T.-M. Lu, S. Lee, Thin Solid Films 516 (2008) 4993.
[19] S.W. Kang, S.K. Mohanta, Y.Y. Kim, H.K. Cho, Cryst. Growth Des. 8 (2008) 1458.
[20] L. Vayssieres, Adv. Mater. 15 (2003) 464.
[21] D.S. Boyle, K. Govender, P. O'Brien, Chem. Commun. 1 (2002) 80.
[22] S. Yamabi, H.J. Imai, Mater. Chem. 12 (2002) 3773.
[23] M. Guo, P. Diao, S.J. Cai, Solid State Chem. 178 (2005) 1864.
[24] K. Govender, D.S. Boyle, P.B. Kenway, P.J. O'Brien, Mater. Chem. 14 (2004) 2575.
[25] L.E. Greene, B.D. Yuhas, M. Law, D. Zitoun, P. Yang, Inorg. Chem. 45 (2006) 7535.
[26] Z. Luo, H. Li, H. Shu, K. Wang, J. Xia, Y. Yan, Cryst. Growth Des. 8 (2008) 2275.
[27] G. Xi, K. Xiong, Q. Zhao, R. Zhang, H. Zhang, Y. Qian, Cryst. Growth Des. 6 (2006) 577.
[28] G. Srinivasan, N. Gopalakrishnan, Y.S. Yu, R. Kesavamoorthy, J. Kumar, Superlattices Microstruct. 43 (2008) 112.
[29] F. Cesano, D. Scarano, S. Bertarione, F. Bonino, A. Damin, S. Bordiga, C. Prestipino, C. Lamberti, A.J. Zecchina, Photochem. Photobiol. A 196 (2008) 143.
[30] C. Fauteux, R. Longtin, J. Pegna, D. Therriault, Inorg. Chem. 46 (2007) 11036.
[31] S. Kumar, G.-H. Kim, K. Sreenivas, R.P.J. Tandon, Phys. Condens. Matter 19 (2007) 472202.
[32] A. Bera, D. Basak, Appl. Phys. Lett. 93 (2008) 053102.
[33] J.D. Prades, F. Hernandez-Ramirez, R. Jimenez-Diaz, M. Manzanares, T. Andreu, A. Cirera, A. Romano-Rodriguez, J.R. Morante, Nanotechnology 19 (2008) 465501.